ARTICLE NO. 79-0096R

Optical Properties of Bipropellant Exhaust Constituents Condensed at 77 K

J.A. Roux,* B.E. Wood,† R.E. Alt,‡ D.F. Frazine*
AEDC Division of ARO, Inc., Arnold Air Force Station, Tenn.
A.M. Smith§
University of Mississippi, University, Miss.
and H.E. Scott¶
Arnold Engineering Development Center, Arnold Air Force Station, Tenn.

The infrared spectral transmittance of cryodeposits formed on a 77 K germanium substrate by MMH, N_2O_4, N_2H_4, and the exhaust plume products from a 5-lb_f (22.25 N) bipropellant engine were measured. The spectra and optical properties for constituents cryopumped at 20 K have previously been presented. However, the deposits formed at 77 K were found to have higher densities and stronger absorption bands, although fewer species cryopump at 77 K. Transmission spectra of cryocontaminant thicknesses from 0.25 μm to 6 μm were obtained for the 500- to 3700-cm^{-1} range using a Fourier transform spectrometer. Values of the refractive index and absorption index (n, k) for bipropellant deposits were derived from the experimental data using an analytical model in conjunction with a nonlinear least-squares method. Results from the least-squares method were also compared with a subtractive Kramers-Kronig determination of the refractive index. A quartz crystal microbalance along with a two-angle laser interference technique was used to measure the cryofilm thickness and density.

Nomenclature

d_l = thin film thickness, μm
f = QCM oscillation frequency, Hz
I = mass flux per unit solid angle, g/s-sr
k = absorption index
K = QCM calibration constant = 1.77×10^{-8} g/cm^2 – Hz
$\dot{m}$ = mass rate collected by QCM, g/s
m_a = order of interferences for incidence angle θ_a
n = real part of refractive index
N = number of engine firing pulses
P_c = combustion chamber pressure, psia (atm)
QCM = quartz crystal microbalance
R = distance from nozzle exit to QCM crystal, cm
t_l = time at which data were recorded, s
t_p = pulse length, s
T_x = QCM crystal temperature, K
β = ratio of interference periods
δ = duty cycle, percent of time engine is pulsed to total time
θ_a = incidence angle, deg
θ_b = incidence angle, deg
λ = wavelength, μm
ν = wavenumber, cm^{-1}
Ω = solid angle subtended by QCM field of view, sr

Received Jan. 5, 1979; presented as Paper 79-0096 at the AIAA 17th Aerospace Sciences Meeting, New Orleans, La., Jan. 15-17, 1979; revision received May 9, 1979.

Index categories: Fuels and Propellants, Properties of; Thermophysical Properties of Matter; Experimental Methods of Diagnostics.

*Research Engineer.
†Research Engineer. Associate Fellow AIAA.
‡Project Engineer.
§Dean of Engineering; formerly Research Supervisor, ARO, Inc. Associate Fellow AIAA.
¶Physicist. Member AIAA.

Introduction

THE potential contamination of spacecraft surfaces and components by exhaust products from spacecraft thrusters—whether solid, liquid, or electric—is of considerable concern to the spacecraft design community. This concern is attributed to the development of more sophisticated spacecraft systems designed to perform multiple noninterfering missions for longer periods of time in space. Contamination and subsequent degradation of sensitive spacecraft surfaces and components, such as thermal control coatings, solar cells, antennas, optical devices, and cooled infrared sensors, can compromise mission objectives and lead to a reduction in spacecraft lifetime. For example, contamination of surfaces with low absorptivity-to-emissivity (α/ϵ) properties, required for passive control of spacecraft temperatures, can result in a heat imbalance with a subsequent change in spacecraft temperature, thus affecting the spacecraft mission and/or lifetime.

In order to predict the effects of rocket exhaust plumes from liquid bipropellant and monopropellant engines on spacecraft surfaces of interest, computer codes have been developed. The codes have been available for several years, but have received only limited use, primarily because of the programming complexity of the codes, but also because of a lack of verifications with representative engine data. The codes are also deficient in the prediction of mass flow outside the nozzle Prandtl-Meyer expansion angle, because the codes do not incorporate any sort of boundary-layer model.

Verification of the accuracy of these codes will require comparisons of predictions to representative measured data. Monopropellant engine data have been obtained previously[1,2] and some of the bipropellant data are included in this paper. These data are important for assessing the potential contamination from the Space Transportation System's (STS) 25-lb_f (111.25 N) and 500-lb_f (2225 N) thrust bipropellant engines. The engine selected for the test described here was a 5-lb_f (22.25 N) thrust bipropellant engine.

This paper contains some of the results for condensed gases at 77 K, which were considered as potential contaminants, as well as the actual cryopumped plume exhaust gases from the

5-lb_f (22.25 N) engine. Since unreacted propellants are considered as contaminants, the propellants MMH, N_2O_4, and N_2H_4 were studied in a research cell in order to prepare for the actual engine firing. The infrared spectral transmittance of MMH and N_2O_4 were measured in a research chamber in order to identify these species in the exhaust plume; N_2H_4 was also studied to gather background information for future monopropellant engine testing. These spectra were measured using an interferometer spectrometer. Also measured were the thickness and density; these were measured using a two-angle laser interference technique and a quartz crystal microbalance (QCM). Having made these property measurements in a small research cell, this same instrumentation was employed at a large test cell to measure these same properties on the 5-lb_f (22.25 N) bipropellant engine. For the 5-lb_f (22.25N) engine, the optical properties (n,k) of the cryopumped (77 K) exhaust species were derived from the transmittance data using a thin-film analytical model in conjunction with a nonlinear least-squares convergence technique and the subtractive Kramers-Kronig method.

Apparatus

Test Unit: Aerospace Research Chamber 10V

The test program was conducted in the Aerospace Research Chamber 10V of AEDC. This chamber is designed for testing small rocket engines under space vacuum conditions. The stainless steel chamber is 10 ft (3.05 m) in diameter, 20 ft (6.1 m) long, and is equipped with an internal cryogenic system designed for high-efficiency vacuum pumping of rocket exhaust products.

Chamber pumpdown is accomplished with mechanical vacuum pumps and a 6-in. (15.2-cm) diffusion pump. Free expansion of the rocket plume is made possible by the high capture rate (pumping speed) of the exhaust gases on the chamber cryogenically cooled surfaces. The chamber cryogenic system consists of a liquid nitrogen (LN_2) cooled (77 K) chamber liner, and a radial finned gaseous helium (GHe) cooled (20 K) cryopump. The chamber configuration for the bipropellant contamination program is shown in Fig. 1.

The 5-lb_f (22.25 N) rocket engine was located at the front of the chamber and fired axially along the chamber horizontal centerline. Engine installation and positioning was performed by means of an antechamber which extends through a penetration on the front of the chamber. The LN_2 cooled surfaces, in the form of a 9-ft (2.74-m) diameter cylinder, line the entire length of the chamber. Several cutouts in the liner exist for visual and physical access to the chamber interior. The radial finned GHe cooled cryopump, approximately 6 ft (1.83 m) in inner diameter, extends nearly the entire length of the LN_2 liner. The circular region at the far end of the chamber is covered with a liquid-nitrogen-cooled shield, while the region at the front of the chamber, between the antechamber and the LN_2 liner is covered with a GHe cooled shield. The LHe cooled cryopump is on the chamber vertical axis at the far end of the chamber.

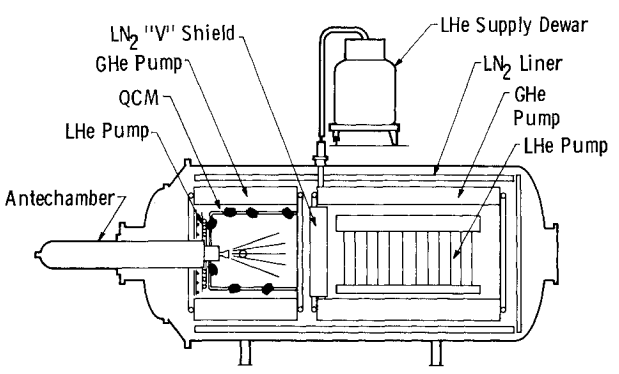

Fig. 1 AEDC 10V cryogenic chamber.

A chamber background pressure of approximately 1×10^{-5} Torr ensured that the plume expansion was not significantly different than would occur in an operational space environment. Also, the molecular mean free path was long enough to permit molecules to travel from the nozzle to the QCM without being deflected by intermolecular collisions. Background gas in the chamber during the pulse firing was primarily H_2 since the pumping speed of the LHe surfaces for H_2 was considerably less than the pumping speed of the GHe surfaces for N_2 and CO or the LN_2 surfaces for CO_2 and H_2O, the other primary gas species in the plume of a bipropellant engine.

Chamber instrumentation used to assess the chamber performance during engine firings were four ionization gages, three glass envelope gages located in the test volume, and a single nude gage located behind the GHe shield in the front of the chamber. The gage mounted on the top end of the antechamber was directed downstream along the plume axis; the gage at the bottom of the chamber faced in the opposite direction toward the GHe shield panel. The third gage in the test volume was attached to a mechanical feedthrough rod, which allowed it to be translated parallel to the plume axis and rotated about its axis.

5-lb_f (22.25 N) Thrust Engine

The 5-lb_f (22.25 N) thrust bipropellant engine was designed to operate on nitrogen tetroxide (N_2O_4) oxidizer and monomethylhydrazine (MMH) ($CH_3N_2H_3$) fuel at a mixture ratio of 1.6 kg N_2O_4/ 1 kg of MMH at propellant supply temperatures between 20° and 120°F (−6.7-48.9°C). The engine was designed to provide high pulse mode performance and low contaminant generation. It should be noted that contaminant in the sense stated here refers primarily to the expulsion of raw propellant, fuel or oxidizer, in either liquid or gaseous form, from the combustion chamber along with the products of combustion. However, since any exhaust product of the engine is capable of contaminating a specific surface (at least in the sense of altering the surface optical or radiative characteristics) all plume gases are loosely referred to as contaminants in this paper.

The baseline engine designated for this program was optimized for maximum performance with a pressure regulated propellant feed system and a combustion chamber-nozzle that was free to radiate (uninsulated). The baseline engine incorporated a six-element splash plate injector (45-deg element orientation) and a 2 in. (5.08 cm) long combustion chamber of cylindrical configuration with a 100:1 expansion ratio nozzle. This engine had no firing or duty cycle limitations at combustion chamber pressures to 110 psia (7.48 atm) and could also operate over a wide range of duty cycles at combustion chamber pressures up to 150 psia (10.2 atm).

Instrumentation

A schematic view of the experimental apparatus showing the IR interferometer (Digilab Model FTS-14), the two laser beams, the high vacuum chamber (10V) containing the cryocooled QCM (#4) and germanium window, and the IR source location is given in Fig. 2. For the bipropellant engine the exhaust products were collected at an angle of 90 deg from the plume axis centerline and at a distance of 32.3 in. (82 cm) along the nozzle exit plane. Normal absolute transmission spectra were measured using 77 K germanium as a substrate material. To minimize the 300 K background radiation seen by the spectrometer, a cold stop was located in the "back-of-window" gas baffle. This stop was 1.50 in. (3.81 cm) in diameter, and the clear aperture of the germanium was 2.0 in. (5.08 cm) in diameter; the germanium window was mounted as shown in Fig. 2. Gas was prevented from condensing on the

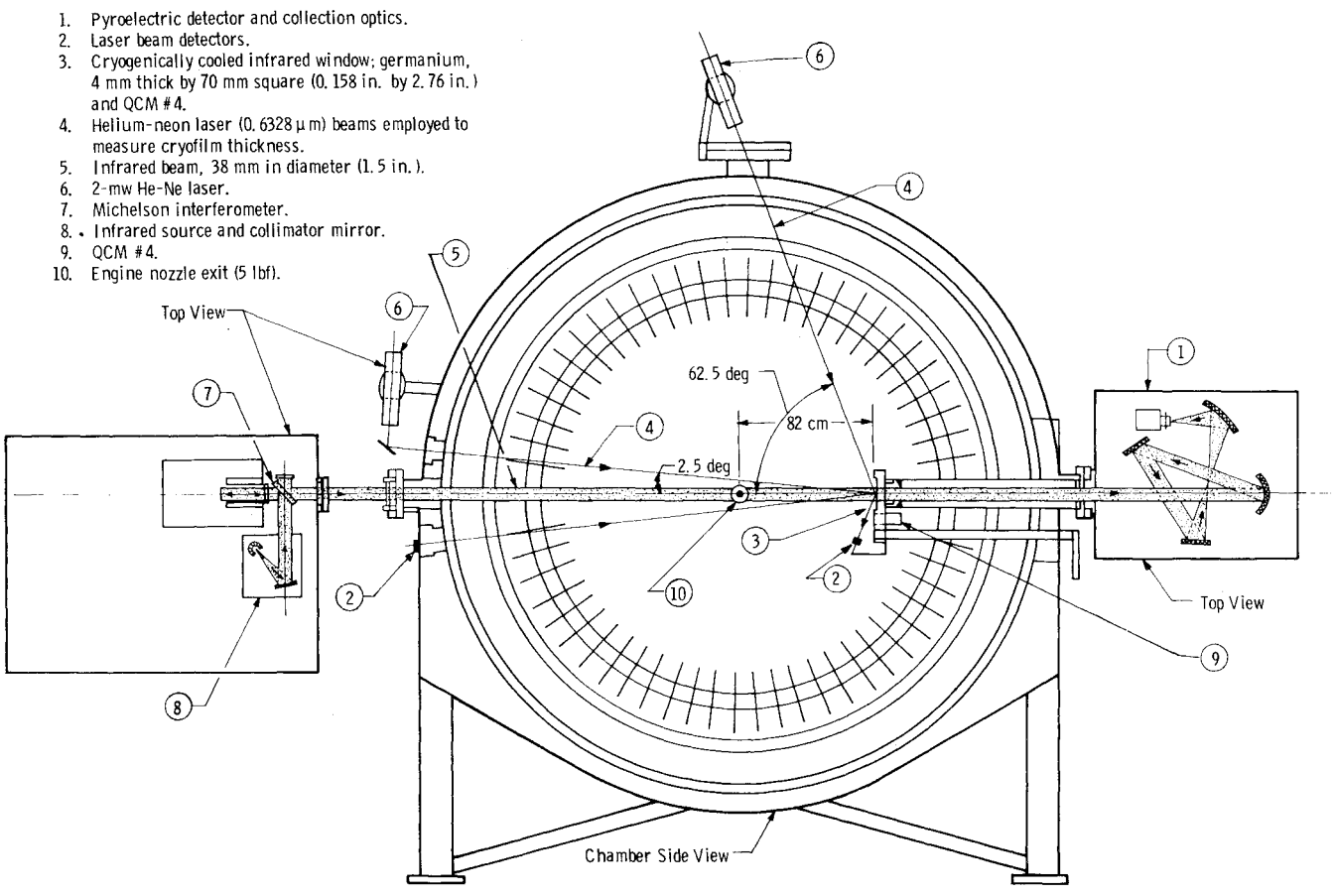

Fig. 2 Schematic of 10V with FTS-14 interferometer, two-angle laser interference apparatus, IR substrate (germanium), and QCM #4.

back of the germanium window by a baffle positioned close to the back of the window holder; this baffle also held the optical stop.

The spectral resolution of the interferometer system could be selected between 16 and 0.5 cm^{-1}; but 4 cm^{-1} resolution proved to be sufficient for the low temperatures where all rotational structure was eliminated. The wave number accuracy of the interferometer is about 0.005 cm^{-1}, limited only by the uncertainty in the optical path difference monitored by the auxiliary He-Ne laser interferometer. Transmission data were recorded in the 500-3500 cm^{-1} (500-3700 cm^{-1} for the research cell) region using a pyroelectric detector. Transmission measurements were performed by rotating the germanium out of the beam and recording and storing a reference power spectrum. A total of 36 interferograms (16 for the research cell) were generally co-added before execution of the Fourier transform, thereby improving the S/N ratio. Next the window was rotated into the beam and the process repeated. The reference file was then divided into the sample file via a NOVA 4001 minicomputer and the ratio plotted by a digital incremental plotter, producing the final data recorded on a linear ordinate scale of 0-100% transmission; these data were also stored on digital tape for further processing by the IBM 370/165 computer to determine optical properties from the transmission data.

The IR transmission of condensed exhaust products collected on the 77 K optical substrate (germanium) was used to provide in situ identification of species deposited on the QCM and to determine optical properties of the condensed exhaust gases. The QCM was located directly below the substrate and was maintained at the same temperature; the QCM was used in conjunction with the IR transmission measurements and the laser interference measurements to obtain the deposit density and thickness. A theoretical model of substrate plus film transmission was developed and subsequently employed with the experimental results to determine the complex refractive index ($\bar{n}=n-ik$) of the cryopumped exhaust constituents.

A two-angle laser interference technique was employed to measure the film thickness and also the film refractive index at 0.6328 μm.[3] Basically, two He-Ne laser (2 mW) beams (Fig. 2) were specularly reflected off the germanium window at different incidence angles (accurate to within 0.5 deg). As the exhaust gases were condensed, two interference fringes of different periods were observed on silicon solar cell detector outputs used to measure the intensity of reflected laser light. If the ratio of the fringe periods is termed β, the refractive index of the film is given by

$$n=\frac{(\sin^2\theta_b-\beta^2\sin^2\theta_a)^{1/2}}{(1-\beta^2)^{1/2}} \tag{1}$$

where θ_a and θ_b (typically 2.5 and 62.5 deg) are the two laser beam incidence angles. Once n has been established, the thickness d_l of the film is readily calculated from $m_a\lambda=2nd_l[1-(\sin^2\theta_a/n^2)]^{1/2}$, where m_a is the order of the interference maxima for incidence angle θ_a. A QCM was used in conjunction with the two-angle laser technique to determine the density of the condensed exhaust products. The laser beams were incident on the center of the same optical substrate used for the IR transmission measurements and thus provided properties for the same deposit. The QCM crystal was mounted on a temperature controlled heat sink connected to the QCM mounting block by a thermal conductor sized to allow 20 K to 300 K temperature cycling in one hour with a heater power of 10W. With these two modifications, the QCM can be clamped to a constant low-temperature 20 K heat sink, the crystal temperature controlled anywhere between the heat sink temperature and 300 K, and the oscillator electronics maintained at room temperature. The QCM crystal was cut

(A-T cut) at 39 deg, 49 min for a low-temperature coefficient in the 77 K range.

Crystal temperature was taken to be that measured by a thermocouple imbedded in the heat sink to which the crystal was mounted. The temperature of the QCM surroundings was less than 80 K, excluding the thruster nozzle directly in the field of view of the QCM, and as a result of radiation exchange between the QCM and its surroundings, the crystal temperature was calculated to be within 0.4 K of the heat sink temperature.

When the QCM crystal had stabilized at the desired temperature (77 K), the QCM frequency and temperature were recorded; this was usually about 10 min prior to the beginning of a sequence of engine firings. A second pair of readings was recorded just prior to the engine firing and a third pair just after the firing sequence. If the data sets are designated 1, 2, and 3, respectively, the measured mass flux I is

$$I = \frac{d\dot{m}}{d\Omega} = \frac{KR^2\Delta f}{Nt_p} \quad \text{g/s-sr} \tag{2}$$

where

$$\Delta f = (f_3 - f_2) - (f_2 - f_1)\frac{t_3 - t_2}{t_2 - t_1} \quad \text{Hz} \tag{3}$$

The second term in Eq. (3) was used to separate the chamber background mass flux from the engine mass flux.

During the firing sequence the QCM frequency was monitored with a frequency-to-voltage converter and a strip chart recorder. If the QCM stopped oscillating due to mass saturation, normally at a frequency between 50 and 100 KHz, the crystal was heated to 300 K to remove the deposit. This process of cleaning the QCM crystal required a maximum of one hour.

Results

It is believed that some of the exhaust species associated with bipropellant engines are due to either unburned MMH or N_2O_4 (N_2H_4 for a monopropellant engine). For identification purposes, the low-temperature IR spectra of MMH, N_2O_4, and N_2H_4 were measured with the same instrumentation but in a research vacuum chamber.

MMH Deposited at 77 K

Thin films of MMH were deposited on LN_2-cooled germanium and transmission spectra were obtained at each laser interference maxima. The refractive index at 77 K and $\lambda = 0.6328$ μm was 1.47 ± 0.02, the density was 0.98 g/cm^3 and the Lorentz-Lorenz constant was 0.284 cm^3/g. For the transmission measurements, film thicknesses up to 40 interference maxima thick (8.84 μm) were deposited and the spectra recorded. Figure 3 shows the spectra obtained for a thickness of 8.84 μm, which was representative of the results obtained. The band locations and assignments are essentially the same as given in Table 1 for the 20 K spectra.[4,5] Essentially all of the bands observed at 77 K are within 10 cm^{-1} of the corresponding bands observed at 20 K.

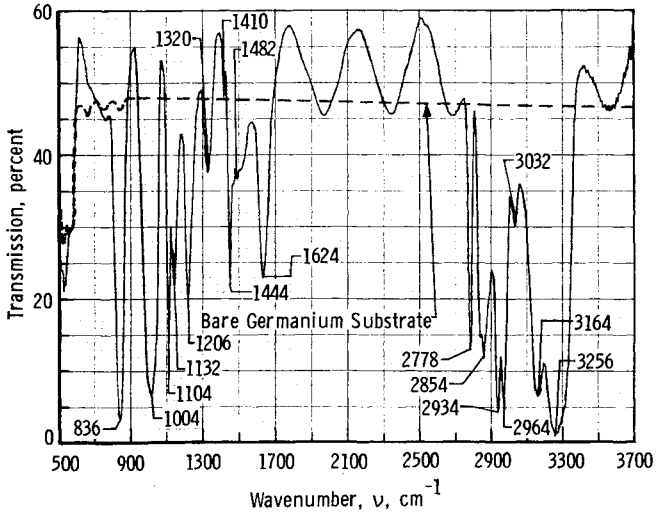

Fig. 3 Transmission of an 8.84-μm-thick MMH cryodeposit on 77 K germanium.

N_2O_4 Deposited at 77 K

Thin films of N_2O_4 were condensed at 77 K. For $\lambda = 0.6328$ μm, the refractive index was determined to be 1.55 ± 0.02 and the density was 2.01 g/cm^3. These values yield a Lorentz-Lorenz constant of 0.159 cm^3/g, which is in only fair agreement with the value of 0.171 cm^3/g obtained for the 20 K measurements.[4] No fracture problems were encountered for the N_2O_4 deposited at this higher temperature. During warmup the N_2O_4 started evaporating at approximately 150 K and a chamber pressure of about 1×10^{-6} Torr.

The infrared transmission spectra for a 4.18 μm thick N_2O_4 film condensed at 77 K is shown in Fig. 4. Bands at 1740 and 1760 cm^{-1} are very intense, also bands at 1255 cm^{-1} (ν_{11}) and the double band at 740 and 760 cm^{-1} are very strong. (see Ref. 6.). The latter band existed as a single band located at 750 cm^{-1} when deposited at 20 K,[4,6] but the splitting was observed later when the films were warmed up. A weak band is observed at 1460 cm^{-1} ($2\nu_7 + R$) and a sharp band at 1620 cm^{-1}. A very sharp narrow band is observed at 1700 cm^{-1} (ν_5) and the strong double band is located at 1740 (ν_9) and 1760 cm^{-1} ($\nu_9 + R$). The remainder of the bands are relatively weak and are located at 1840, 2240, 2340, 2580,

Table 1 MMH cryodeposit band assignments

Wavenumber					
20 K	After warmup to 160 K	77 K	After warmup to 161 K	Liquid[5] MMH	Assignment
836	845	840	835	814	ν_{18}
	860		860		
1004	985	1015	1010	985	ν_{16}
1104	1105	1105	1120	1094	ν_{15}
1132	1130	1140	1140	1120	ν_{13}
1206	1220	1220	1220	1194	ν_{12}
1320	1350	1335	1345	1295	ν_{11}
1410	1410	1415	1405	1411	ν_{10}
1444	1450	1450	1440	1438	ν_9
			1460		
1482	1480	1480	1490	1472	ν_8
1624	1620	1630	1620	1608	ν_7
			1700		
			1850		
			2020		
			2060		
			2140		
			2210		
			2340		
			2660		
2778	2795	2780	2780	2784	ν_6
2854	2865	2860	2860	2858	$\nu_9 + \nu_{10}$
2934	2945	2940	2940	2937	ν_5
2964	2990	2980	2980	2963	ν_4
3032		3020	3020		$\nu_7 + \nu_{10}$?
3164	3165	3160	3140		$\nu_3 + \nu_{11} - \nu_{10}$?
3256	3260	3260	3215	3250	ν_3
	3360		3340		ν_1 or ν_2?

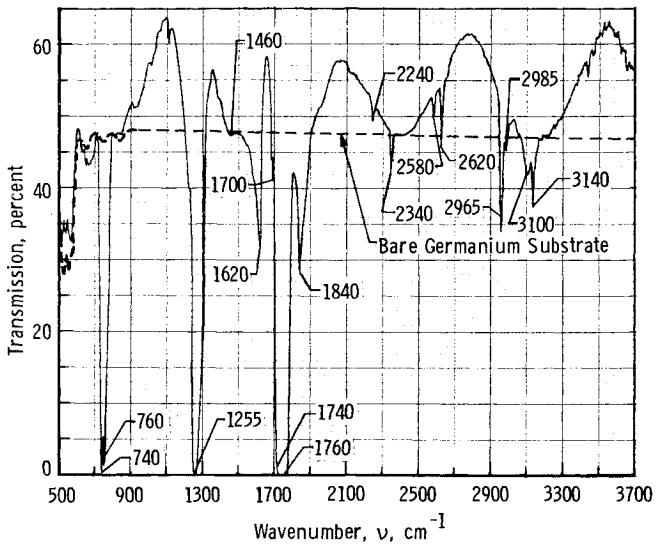

Fig. 4 Transmission of a 4.18-μm-thick N_2O_4 cryodeposit on 77 K germanium.

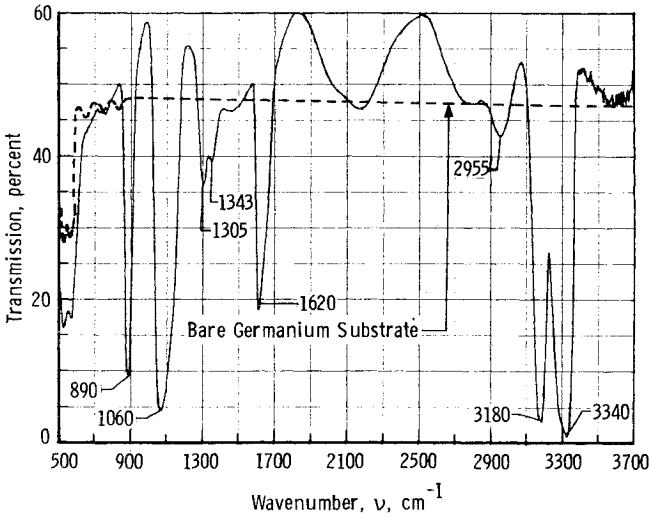

Fig. 5 Transmission of a 4.63-μm-thick N_2H_4 cryodeposit on 77 K germanium.

2620, 2965 ($\nu_5+\nu_{11}$), 2985, 3100 ($2\nu_7+\nu_9$), and 3140 cm^{-1} ($2\nu_7+\nu_9+R$).

Hydrazine (N_2H_4) at 77 K and 20 K

The other fuel studied was hydrazine (anhydrous) which is a monopropellant. A sample was collected from a fuel drum of N_2H_4 and a chemical analysis showed the composition (by weight) to be $N_2H_4=99.2\%$, $H_2O=0.6\%$, and amines $=0.2\%$.

Deposition was first attempted for the germanium window cryogenically cooled to 20 K. However, only a few (2-6) interference maxima were obtained before dying out due to a fracture-type phenomenon. This phenomenon sometimes occurred as a sudden fracture with the immediate cessation of the interference pattern or as a rapid deterioration of the interference pattern quality. The spectra of these deposits before fracturing, however, were not unlike that obtained for the 77 K measurements, so they won't be presented here. With the germanium window at 77 K, hydrazine films up to 32 interference maxima thick were obtained before fracture occurred. The refractive index at $\lambda=0.6328$ μm was found to be 1.51 ± 0.02 and the density was 1.17 g/cm^3 at 77 K. These values yield a Lorentz-Lorenz constant of 0.253 cm^3/g at this wavelength. At a chamber pressure of 3×10^{-6} Torr, the hydrazine films evaporated between 180 and 190 K.

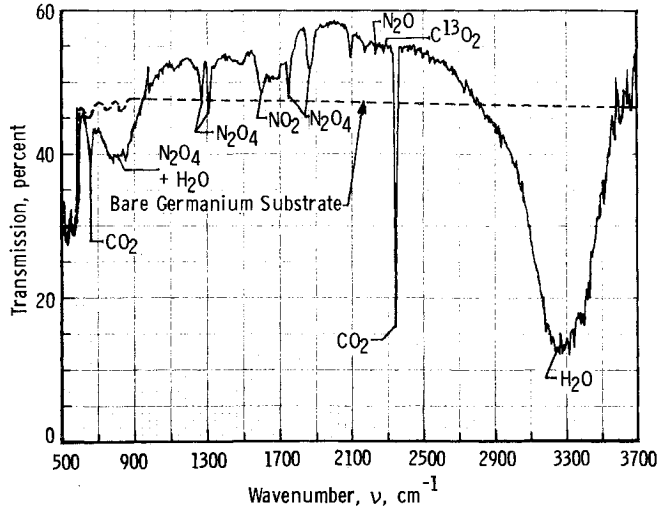

Fig. 6 Transmission of a 0.89-μm-thick (fourth laser interference maximum) deposit from bipropellant engine condensed on 77 K germanium.

The transmission spectra of hydrazine formed on 77 K germanium is shown in Fig. 5. Locations of the major absorption bands are at 890, 1060, 1305, 1345, 1620, 2955, 3180, and 3340 cm^{-1}. Some of these bands agree with previously published data[5] obtained on solid hydrazine such as the 3340, 3180, and 890-cm^{-1} bands. The relatively weak band at 2955 cm^{-1} was also observed in Ref. 5, but was not identified. The two weak bands at 1305 and 1345 cm^{-1} were observed in Ref. 5 but the relative intensities were reserved. The data of Ref. 5 were also obtained for N_2H_4 condensed at LN_2 temperatures but in a gas cell. Although it wasn't stated in Ref. 5, the deposits are believed to have been condensed at a relatively high pressure and formed in the crystalline phase. The N_2H_4 deposits formed in this study were condensed at a chamber pressure of approximately 1×10^{-7} Torr and were of the amorphous form. As such, the spectra may be representative of a supercooled liquid as contrasted to a crystalline solid.

Identification of Species Condensed at 77 K

Transmission measurements of cooled germanium and contaminants from the engine were made for condensates formed at 77 K as opposed to the previous 26 K temperature.[4] Gases such as O_2, N_2, CO, CH_4, and NO would not be expected to condense at the higher temperature (77 K) due to their higher vapor pressure. Gases such as H_2O, CO_2, NO_2, N_2O_4, N_2O, MMH, and possibly N_2O_3 should be the major constituents condensable at 77 K. Transmission measurement results for 77 K are shown in Fig. 6 (Fig. 7 for 26 K is shown for comparison purposes) for a deposit thickness of 0.89 μm. The two narrow bands located at 2340 and 660 cm^{-1} are the ν_3 and ν_2 CO_2 bands, respectively, whereas the broad bands observed between 700-900 cm^{-1} (approximately 720-790 cm^{-1}) are due to the N_2O_4 (ν_{12}) band which occurs as a strong doublet band between 740-760 cm^{-1} as was observed for pure N_2O_4 condensed at 77 K.

The N_2O_4 bands at 1265 and at 1305 cm^{-1} were both observed in the bipropellant engine data obtained at 26 K (Fig. 7). At 77 K, however, the band intensities are nearly the same (Fig. 6) whereas the 1305-cm^{-1} band was much stronger than the 1265-cm^{-1} band for the 26 K[4] bipropellant data. Upon warmup to 124-134 K (Fig. 8) the band intensities changed with the 1265-cm^{-1} band becoming as strong as or stronger than the 1305-cm^{-1} band. For pure N_2O_4 deposited at 77 K (Fig. 4), the band at 1305 cm^{-1} was not observed at all, but it was observed when condensed at 20 K[4]. It,

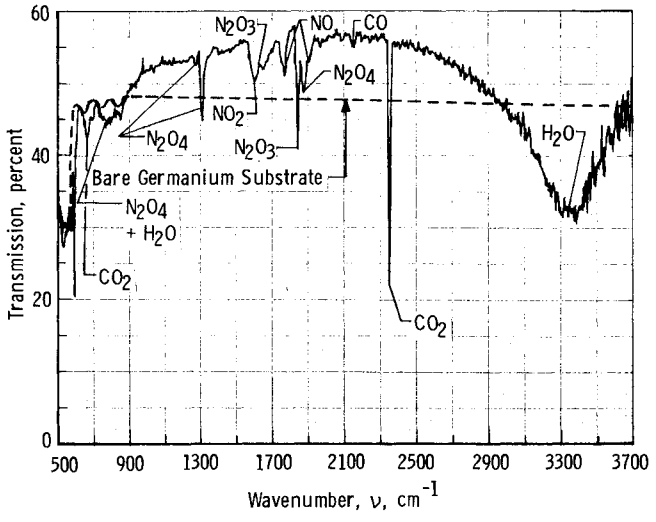

Fig. 7 Transmission of a 0.94-μm-thick (fourth laser interference maximum) deposit for bipropellant engine condensed on 26 K germanium.[4]

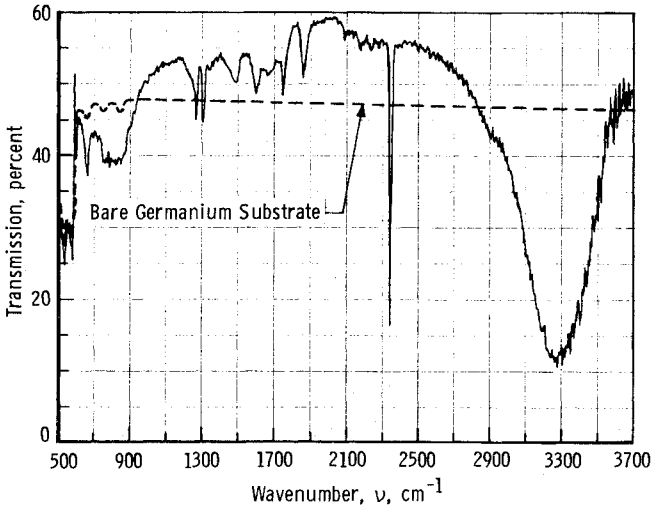

Fig. 8 Transmission of a 0.89-μm-thick deposit from bipropellant engine that was formed at 77 K and subsequently warmed up to 124-134 K.

therefore, appears that the existence of this band at 1305 cm^{-1} is very temperature dependent. (Note: It is also possible that this band could be correlated with the existence of N_2O_3.)

The band which occurs at 1600 cm^{-1} (Fig. 6) is the NO_2 ν_3 band which was observed in both the exhaust plume and N_2O_4 data condensed at 26 K (Fig. 7). The band which occurs at 1745 cm^{-1} is the N_2O_4 ν_9 band. Similarly, the band near 1870 cm^{-1}, the $\nu_4+\nu_5$ band of N_2O_4, was also seen in the N_2O_4 and bipropellant data for condensation at 20-26 K[4] and for the N_2O_4 deposited at 77 K. The next absorption band in Fig. 6 (progressing in the direction of greater wavenumbers) is located at 2090-2100 cm^{-1}. This unidentified band was also observed in 26 K exhaust plume data[4] but was not seen for N_2O_4 deposited at either 77 K or 20 K. This may be the $\nu_1+\nu_{12}$ band of N_2O_4 (Ref. 6) which is relatively weak even in the gas phase and may only show up when isolated within a matrix of other condensed gases. The other most probable candidate would be the ν_3 cyanogen (C_2N_2) band which occurs at 2150 cm^{-1} in the gas phase. The identity is still uncertain as the band shows up relatively weak in Fig. 6 and may represent only a trace amount. Thicker deposits would have aided in the identification of this species.

The final bands observed in Fig. 6 are a series of three weak bands between 2100 and 2300 cm^{-1} which occur at approximately 2175, 2240, and 2280 cm^{-1}. The very weak band at 2175 cm^{-1} also is not identified but remained until the deposit was warmed up to 200 K under vacuum and the N_2O_4 had already evaporated. The other two bands located at 2240 and 2280 cm^{-1} are attributed to N_2O and $C^{(13)}O_2$, respectively.

Gas Phase Transmission Data

During the chamber warmup the germanium substrate was rotated out of the IR beam, enabling the 10V chamber to be used as a large absorption cell for identifying the gas species which sublimated during chamber warmup. Each gas spectrum in Fig. 9 was recorded with the FTS-14 at a resolution of 1 cm^{-1} and by co-adding 64 scans. Also, each spectrum was normalized by the spectrum recorded while the chamber was cold and pumped down to 10^{-6} Torr. The chamber pressure (Torr), the GHe panel temperature, and the LN_2 panel temperature are shown at the lower left-hand corner of each figure. The chamber was allowed to warm up at its own rate without providing additional heat, except at Fig. 9h the chamber was pressurized from 48 mm up to 500 mm with dry N_2 gas which did provide extra heat. The LN_2 panels warmed slower than the GHe panels because of the remaining liquid nitrogen in the lines which required more heat to evaporate.

In Fig. 9a, CO was immediately observed as the temperature of the GHe panels reached 55 K. The strong CO band indicated a significant volume of CO evaporated during warmup; however, in the backflow region only a trace amount of condensed CO had been detected in the 26 K IR spectrum. Upon warming the GHe panels to 105 K (Fig. 9b), methane (CH_4) was clearly seen along with a trace amount of CO_2. Methane, although seen here in the gas phase, was not detected in the condensed phase at 26 K[4] in the backflow region (similar to CO). The CO_2 became more evident when the GHe and LN_2 panels were warmed to 179 and 142 K, respectively (Fig. 9c). Also, in Fig. 9c, NO, H_2O, N_2O, HCN, ethylene (C_2H_4), and acetylene (C_2H_2) became identifiable.

After the temperature of the GHe and LN_2 panels reached 189 and 155 K, respectively, the NO_2 and $C^{13}O_2$ bands became evident. Further warmup, as shown in Fig. 9, to 210 and 184 K, respectively, revealed the N_2O_4 bands. Additional warmup to 260 and 250 K by pressurizing the chamber to 500 mm with dry nitrogen did not yield any additional observable species, although H_2O, CO_2, N_2O, NO, CO, and CH_4 bands became much more pronounced.

It is interesting to note that in the gas phase CO, CO_2, $C^{13}O_2$, N_2O, NO, NO_2, and N_2O_4 were all identified; these same species were also found in the backflow region (26 K). However, methane (CH_4), HCN, acetylene (C_2H_2), and ethylene (C_2H_4), were also observed in the gas phase; none of these species were found in the backflow IR spectra at 26 K or 77 K. These constituents being seen in the chamber warmup but not seen in the 26 K backflow IR spectra means that these species probably exist in the plume core and thus can only exist in the forward flow region. These species probably do not exist in the nozzle boundary layer and thus do not undergo expansion into the backflow region. However, the more volatile N_2O_4 vapor can diffuse into the nozzle boundary layer where less efficient combustion occurs. The effects of this incomplete combustion is the formation of species such as NO, N_2O, N_2O_3, and NO_2 along with unreacted N_2O_4. These species being in the boundary layer allow for their expansion into the backflow region. Another explanation for some species (CH_4, HCN, C_2H_2, C_2H_4) not existing in the backflow region is that they are not formed in the exhaust plume but are actually formed on the cryopanels during the chamber warmup.

The two relatively strong bands covering the wavenumber ranges from 775-875 cm^{-1} and 960-1060 cm^{-1} in Figs. 9f-9i have not yet been identified. These bands were first seen at GHe and LN_2 panel temperatures of 210 and 184 K,

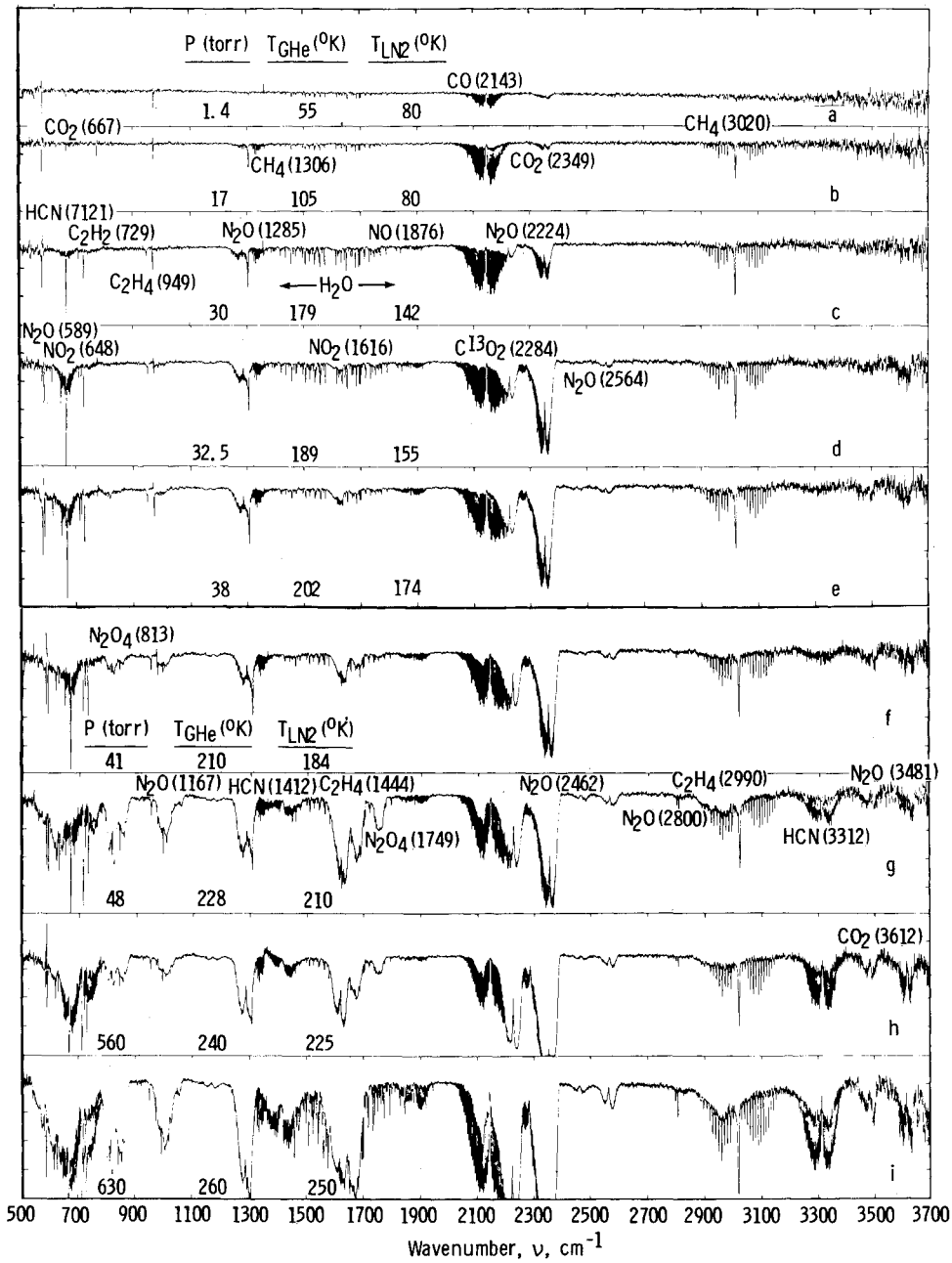

Fig. 9 Gas species identification during chamber warmup.

respectively, for a chamber pressure of 41 Torr. The bands in appearance resemble MMH ($CH_3N_2H_3$) but are shifted considerably in wavenumber and a strong MMH band at 2800-2900 cm^{-1} is not observed in the bipropellant data of Fig. 9. Therefore, MMH was eliminated as the possible source of these bands. Several species similar to MMH in chemical formula were considered such as trimethylhydrazine, trimethlyamine, tetramethyl hydrazine, monomethylamine, monoethylamine, methyl azide, azomethane and others, but none were seen to match. It appears that these two bands are due to some modified form of the MMH molecule.

Optical Constants

In order to determine the complex refractive index ($\tilde{n}=n-ik$) of the thin solid exhaust plume film from the IR transmission measurements for wavenumbers between 700 and 3500 cm^{-1}, an analytical model of film plus window transmission was used. The optical constants of the cryocontaminants were determined by using this analytical transmission model[7,8] in conjunction with a nonlinear least-squares convergence routine. Also, the subtractive Kramers-Kronig relation between n and k was used in conjunction with the nonlinear least-squares determination of n. The subtractive Kramers-Kronig relation is given by

$$n(\nu)=n(\nu_m)+\frac{2}{\pi}P\int_0\left[\frac{k(\nu')\nu'-k(\nu)\nu}{(\nu')^2-\nu^2}-\frac{k(\nu')\nu'-k(\nu_m)\nu_m}{(\nu')^2-\nu_m^2}\right]d\nu' \quad (4)$$

where ν_m is a reference frequency (2180 cm^{-1}) and P indicates the Cauchy principal value of the integral. Integration was performed using the simple trapezoidal rule; the k values used in Eq. (4) were those determined by the nonlinear least-squares technique. The transmission data recorded for all deposits discussed here were digitized every 2 cm^{-1}.

Usually a minimum of 15 thicknesses (laser interference maxima) is desired in order for the analytical model to converge upon a well defined value of n. The n value appears

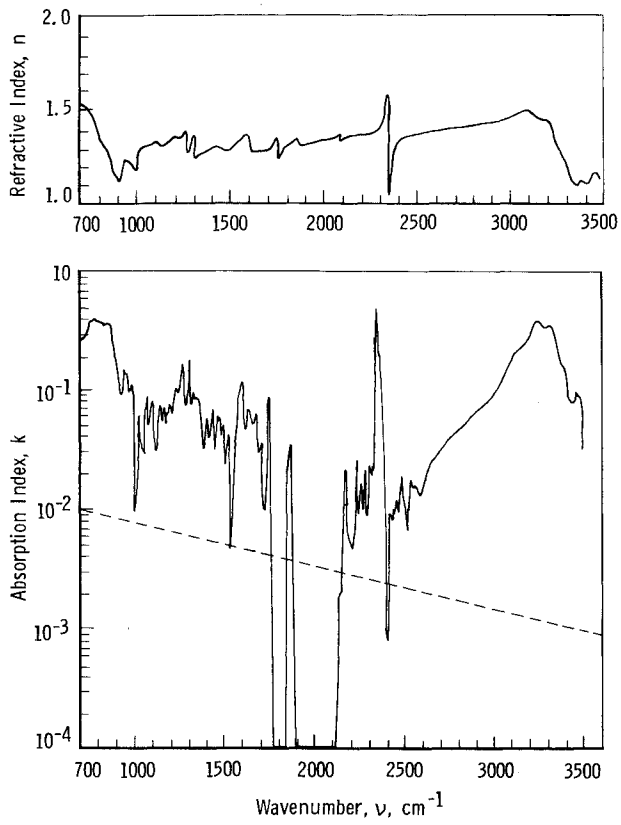

Fig. 10 Optical properties for bipropellant plume constituents condensed on 77 K germanium.

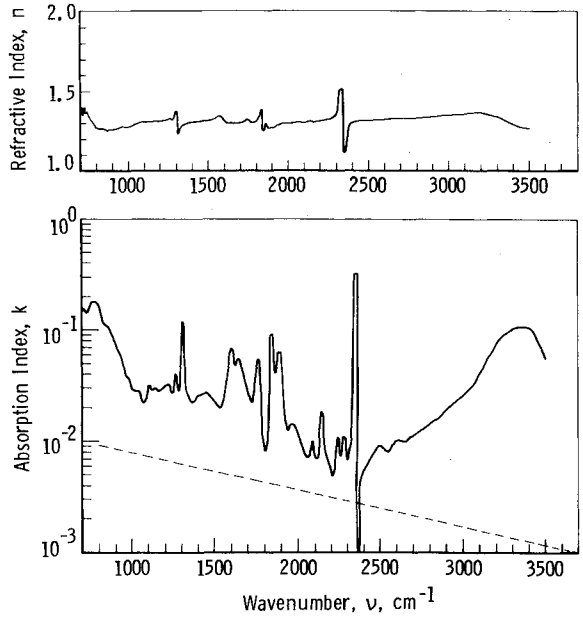

Fig. 11 Optical properties for bipropellant plume constituents condensed on 26 K germanium.[4]

to be defined primarily by the period of the transmission vs thickness curve at each wavenumber. However, the test schedule only permitted time for the formation of four thicknesses at 77 K. When only a few thicknesses are obtained, a transmission vs thickness (for each wavenumber) curve is not well defined. It was found that for the high wavenumbers (>2100 cm^{-1}) the analytical model had no problem in defining n; however, at the lower wavenumbers a neighborhood (range) of n values seemed to satisfy the

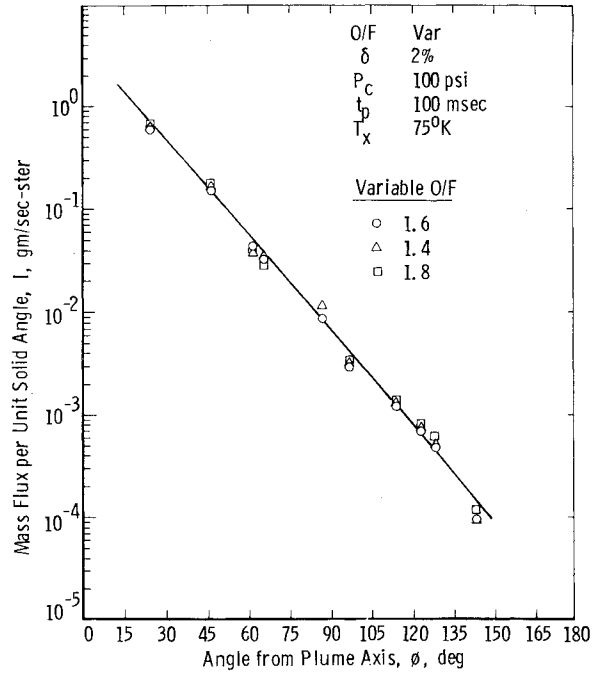

Fig. 12 Mass flux from bipropellant engine as a function of angle from plume axis.

transmission data equally well. The k value, which is primarily determined by the magnitude of the transmission, did not have this difficulty and was well defined over the whole spectral region (700 to 3500 cm^{-1}). Thus, to determine n, the k values were used with the subtractive Kramers-Kronig technique [Eq. (4)] to compute n; these new n values were then used in the analytical model (along with the k values) to see if good agreement occurred with the transmission data. For all wavenumbers the Kramers-Kronig n's along with the least-squares k's yielded excellent agreement when the analytical model and transmission data were compared. The optical constants for the condensed plume constitutents at 77 K are shown in Fig. 10; for comparison the results from Ref. 4 at 26 K are shown in Fig. 11. The dashed lines in Figs. 10 and 11 represent the bounds on the minimum absorption index that can be determined due to the error limits on the film-window transmission measurements. Comparison of Figs. 10 and 11 shows that the absorption index values for the absorption bands are greater at 77 K than at 26 K; also the refractive index values for the 77 K data are slightly greater than the 26 K data. This is partially due to the density difference, i.e., $\rho = 0.76$ g/cm^3 at 26 K and $\rho = 1.01$ g/cm^3 at 77 K.

The optical properties presented are important for calculating the effects of possible deposits upon cryogenically cooled surfaces. Such surfaces as cryogenically cooled sensor optics and telescopes will be functioning in the wavenumber region investigated. The interpretation of information from these types of instruments, when contaminated with thin films, will require spectral knowledge of n and k.

Mass Flux

Not only is it important to identify the contaminating species and their optical properties, but it is also important to be able to predict the mass flux of the contamination. This is necessary so that, for contamination purposes, a specific location on a spacecraft can be determined suitable for a specific piece of optical instrumentation. Also, the mass flux is important to be able to predict the thickness of contamination and how this might affect both performance and life time of optical systems.

In this section a sample of the mass flux results is presented in the form of mass flux per unit solid angle I(g/s-sr) for various operating conditions. The oxidizer-to-fuel ratio (O/F), pulse duty cycle (δ), combustion chamber pressure (P_c), firing pulse length (t_p), and QCM crystal temperature (T_x), are specified in Fig. 12. Mass flux as a function of angle from the plume axis is shown in Fig. 12. The data points correspond to the locations of the QCM's and the solid line represents the best least-squares fit to the data. The mass flux measurements at 90 deg correspond to the same location where the optical measurements were recorded (Figs. 6-8). The data in Fig. 6 correspond to 1300 engine pulses at O/F = 1.6 and t_p = 100 ms, with the QCM (90 deg) located at a distance of 1 m (3.28 ft) from the center of the nozzle engine exit plane. Variation of the engine parameters showed no significant difference from the data shown in Fig. 12; the only parameter causing a significant change, as expected, was crystal temperature.

Summary

Infrared transmission spectra for MMH, N_2O_4, and N_2H_4 condensed at 77 K were recorded, and the spectra for exhaust plume species from a 5-lb_f (2.27-kg_f) bipropellant engine condensed at 77 K were presented. The species in the 77 K cryopumped exhaust plume were identified and the optical properties of the solid phase were determined. Spectra of the chamber warmup were recorded to show the difference between the species identified in the 77 K cryodeposit and those sublimated from the chamber cryoliner.

Acknowledgments

The work reported herein was conducted for the Arnold Engineering Development Center (AEDC), Air Force Systems Command (AFSC), by ARO, Inc., a Sverdrup Corporation Company, operating contractor for the AEDC. This work was sponsored in part by the Air Force Rocket Propulsion Laboratory, Edwards Air Force Base, Calif.

References

[1] Williams, W.D., McCay, T.D., Powell, H.M., Weaver, D.P., Price, L.L., and Lewis, J.W.L., "Experimental Study of Monopropellant Hydrazine Thruster Exhaust," *Proceedings of the 10th JANNAF Plume Technology Conference,* San Diego, Calif., 1977.

[2] McCay, T.D., Weaver, D.P., Williams, W.D., Powell, H.M., and Lewis, J.W.L., "Exhaust Plume Contaminants from an Aged Hydrazine Monopropellant Thruster," *Proceedings of the USAF/NASA International Spacecraft Contamination Conference,* Air Force Materials Laboratory, Wright-Patterson Air Force Base, Ohio, AFML-TR-78-190/NASA-CP-2039, May 1979, pp. 456-517.

[3] Pipes, J.G., Roux, J.A., Smith, A.M., and Scott, H.E., "Infrared Transmittance of Contaminated Cryocooled Optical Windows," *AIAA Journal,* Vol. 16, Sept. 1978, pp. 984-990.

[4] Roux, J.A., Wood, B.E., Smith, A.M., Pipes, J.G., and Scott, H.E., "IR Optical Properties of Bipropellant Cryocontaminants," *Proceedings of the USAF/NASA International Spacecraft Contamination Conference,* Air Force Materials Laboratory, Wright-Patterson Air Force Base, Ohio, AFML-TR-78-190/NASA-CP-2039, May 1979, pp. 412-455.

[5] Durig, J.R., Harris, W.C., and Wertz, D.W., "Infrared and Raman Spectra of Substituted Hydrazines. I. Methylhydrazine," *The Journal of Chemical Physics,* Vol. 50, Feb. 1969, pp. 1449-1461.

[6] Begun, G.M. and Fletcher, W.H., "Infrared and Raman Spectra of $N_2{}^{14}O_4$, and $N_2{}^{15}O_4$," *Journal of Molecular Spectroscopy,* Vol. 4, 1960, pp. 388-397.

[7] Vasicek, A., *Optics of Thin Films,* North Holland Publishing Company, Interscience Publishers, Inc., New York, 1960.

[8] Heavens, O.S., *Optical Properties of Thin Solid Films,* Dover Publications, Inc., New York, 1965.